The Atmospheric Energy Budget and Large-Scale Precipitation Efficiency of Convective Systems during TOGA COARE, GATE, SCSMEX, and ARM: Cloud-Resolving Model Simulations

W.-K. TAO

Laboratory for Atmospheres, NASA Goddard Space Flight Center, Greenbelt, Maryland

D. JOHNSON AND C.-L. SHIE

Laboratory for Atmospheres, NASA Goddard Space Flight Center, Greenbelt, and Goddard Earth Sciences and Technology Center, University of Maryland, Baltimore County, Baltimore, Maryland

J. SIMPSON

Laboratory for Atmospheres, NASA Goddard Space Flight Center, Greenbelt, Maryland

(Manuscript received 3 October 2002, in final form 28 April 2004)

ABSTRACT

A two-dimensional version of the Goddard Cumulus Ensemble (GCE) model is used to simulate convective systems that developed in various geographic locations (east Atlantic, west Pacific, South China Sea, and Great Plains in the United States). Observed large-scale advective tendencies for potential temperature, water vapor mixing ratio, and horizontal momentum derived from field campaigns are used as the main forcing. The atmospheric temperature and water vapor budgets from the model results show that the two largest terms are net condensation (heating/drying) and imposed large-scale forcing (cooling/moistening) for tropical oceanic cases though not for midlatitude continental cases. These two terms are opposite in sign, however, and are not the dominant terms in the moist static energy budget.

The balance between net radiation, surface latent heat flux, and net condensational heating vary in these tropical cases, however. For cloud systems that developed over the South China Sea and eastern Atlantic, net radiation (cooling) is not negligible in the temperature budget; it is as large as 20% of the net condensation. However, shortwave heating and longwave cooling are in balance with each other for cloud systems over the west Pacific region such that the net radiation is very small. This is due to the thick anvil clouds simulated in the cloud systems over the Pacific region. The large-scale advection of moist static energy is negative, as a result of a larger absolute value of large-scale advection of sensible heat (cooling) compared to large-scale latent heat (moistening) advection in the Pacific and Atlantic cases. For three cloud systems that developed over a midlatitude continent, the net radiation and sensible and latent heat fluxes play a much more important role. This means that the accurate measurement of surface fluxes and radiation is crucial for simulating these midlatitude cases.

The results showed that large-scale mean (multiday) precipitation efficiency (PE) varies from 24% to 31% (or 32% to 45% using a different definition of PE) between cloud systems from different geographic locations. The model results showed that there is no clear relationship between the PE and rainfall, the positive cloud condensation (condensation plus deposition), or the large-scale forcing. But, the model results suggest that cases with large, positive net condensation terms in the moist static energy budget tend to have a large PE.

The PE and its relationship with relative humidity and the vertical shear of the horizontal wind are also examined using 6-hourly model data. The model results suggest that there is no clear relationship between the individual PE and total mass-weighted relative humidity or the middle- and upper-tropospheric moisture for each case. The model results suggest that for the west Pacific and east Atlantic cases, PE slightly decreases with increasing middle-tropospheric wind shear in low to moderate shear regimes. The correlation (based on the best polynomial fit) is quite weak however. No strong relationship between PE and wind shear was found for the South China Sea and cases over the United States.

1. Introduction

Cloud-resolving (or cumulus ensemble) models (CRMs) are one of the most important tools used to establish quantitative relationships between diabatic heating and rainfall. This is because latent heating is dominated by phase changes between water vapor and small, cloud-sized particles, which cannot be directly detected. CRMs have sophisticated (though still parameterized) microphysical processes that can simulate the conversion of cloud (liquid and solid) condensate into

Corresponding author address: Dr. Wei-Kuo Tao, Mesoscale Atmospheric Branch, NASA GSFC, Code 912, Greenbelt, MD 20771. E-mail: tao@agnes.gsfc.nasa.gov

raindrops and various forms of precipitation ice. For this reason, CRMs were suggested as one of the primary approaches to improve the representation of moist and other subgrid-scale processes in global circulation and climate models [Global Energy and Water Cycle Experiment (GEWEX) Cloud System Study (GCSS) Science Plan 1994]. Progress in studying ''precipitating convective systems'' in GCSS is reported in Moncrieff et al. (1997).

The use of CRMs in the study of tropical convection and its relation to the large-scale environment can be generally categorized into two methodologies. The first approach is so-called *cloud ensemble modeling.* In this approach, many clouds/cloud systems of different sizes in various stages of their life cycles can be present at any model simulation time. The large-scale effects that are derived from observations are imposed into the models as the main forcing, however. In addition, the cloud ensemble models use cyclic lateral boundary conditions (to avoid reflection of gravity waves) and require a large horizontal domain (to allow for the existence of an ensemble of clouds). The advantage of this approach is that the modeled convection will be forced to almost the same (but not identical) intensity, thermodynamic budget, and organization as the observations. This approach will also allow the CRM to perform multiday or multiweek time integration. This type of cloud-resolving modeling was used by many modeling studies for studying SCSMEX, GATE, TOGA COARE, and DOE/ARM/SGP[1] convective systems (Soong and Tao 1980, 1984; Tao and Soong 1986; Lipps and Hemler 1986; Krueger 1988; Xu and Randall 1996; Wu et al. 1998, 1999; Grabowski et al. 1996, 1998; Das et al. 1999; Li et al. 1999; Donner et al. 1999; Petch and Gray 2001; Xu et al. 2002; Johnson et al. 2002; Tao et al. 2000, 2003a; and others). On the other hand, the second approach for CRMs usually requires initial temperature and water vapor profiles that have a medium to large convective available potential energy (CAPE), and an open lateral boundary condition is used. The modeled clouds, then, are initialized with either a cool pool, warm bubble, or surface processes (Klemp and Wilhelmson 1978; Cotton and Tripoli 1978; Wilhelmson and Klemp 1978; Weisman and Klemp 1982; Fovell and Ogura 1988; Tao and Simpson 1989; Tao et al. 1995, 1996; Ferrier et al. 1996; and many others). Key developments in cloud ensemble modeling using the large-scale forced convection approach over the past two decades were listed by Tao (2003, Table 1).

Precipitation efficiency (PE) is a physical parameter that generally relates the surface rainfall, the large-scale convergence of water vapor, and the microphysical processes (i.e., condensation, evaporation). It also provides needed information for closure assumptions in some cumulus parameterization schemes (i.e., Anthes 1977; Fritsch and Chappell 1980; Grell 1993). Observational studies have estimated the PE associated with thunderstorms (i.e., Braham 1952; Fankhauser 1988) and mesoscale convective systems (i.e., Gamache and Houze 1983; Chong and Hauser 1989; Oury et al. 2000). Please refer to Ferrier et al. (1996) for a review of previous studies and cumulus parameterizations. CRMs have also been used to investigate the PE (Weisman and Klemp 1982; Lipps and Hemler 1986; Ferrier et al. 1996; Lucas et al. 2000; Shepherd et al. 2001). However, these modeling studies only examined the PE associated with an individual cloud or a cloud system, not ensembles of clouds/cloud systems.

Observations of cumulus clouds generally indicate that clouds do not exist as isolated entities but occur in groups or clusters (e.g., Malkus 1957; Lilly 1975; and others). The large-scale models (especially the global circulation models and climate models) need these statistical properties of cloud ensembles under different large-scale environments. Long-term CRM integration using the cloud ensemble modeling approach can simulate the initial, mature, and decaying stages of ensembles of the clouds/cloud systems. The CRM, then, can obtain enough samples to compute the statistical properties of clouds/cloud systems. The PE is termed the ''large-scale'' PE in this modeling study because it is not just associated with one particular cloud or cloud system and also is simulated with the imposed large-scale advective forcing.

The Goddard Cumulus Ensemble (GCE) model is a CRM. It has been used to perform long-term integrations to simulate active convective periods during GATE, TOGA COARE, ARM, and SCSMEX (Das et al. 1999; Li et al. 1999; Johnson et al. 2002; Tao et al. 2003a; and several others). In this paper, the results from the GCE model simulations will be used to calculate the atmospheric (temperature, water vapor, and moist static) energy budgets associated with these convective systems. In addition, the PE associated with these different convective systems will be estimated using the model-simulated energy budget and rainfall. The similarities and differences in the energy budgets and PE between these convective systems are then compared. In section 2, the large-scale environmental conditions associated with these clouds/cloud systems are described. The model and model setup used in the budget calculations are discussed in section 3. The results are shown and discussed in section 4. Finally, the major results and future work are summarized in section 5.

2. Large-scale environmental conditions

The most intense convection during TOGA COARE occurred in middle and late December 1992, prior to

[1] SCSMEX stands for South China Sea Monsoon experiment; GATE stands for Global Atmospheric Research Programme (GARP) Atlantic Experiment. TOGA-COARE stands for Tropical Ocean-Global Atmosphere Program-Coupled Ocean–Atmosphere Response Experiment. DOE/ARM/SGP stands for Department of Energy/Atmospheric Radiation Measurement Program/Southern Great Plains site (in the central United States).

the peak of westerly wind bursts around 1 January 1993. Westerlies started to appear near the surface over the TOGA COARE Intensive Flux Array (IFA) in early December and gradually developed and intensified, although the middle and upper troposphere were still dominated by easterlies. Several major convective events occurred around 11–16 and 20–25 December 1992, mainly due to low-level large-scale convergence of easterlies and westerlies. However, the synoptic conditions were different for these two December events. Easterly flow prevailed at low levels from near the date line westward to the IFA, and convection over the IFA arrived from the east with an easterly surge on 11–16 December. During 21–24 December, there was a greater contribution to heating from stratiform precipitation caused by the increased wind shear (Lin and Johnson 1996). There was less of a stratiform contribution for the 11–16 December convective episode. These two different periods, 10–17 December 1992 and 19–27 December 1992, have been simulated using the two-dimensional (2D) version of the GCE model (Das et al. 1999; Tao et al. 2000; Johnson et al. 2002). The large-scale forcing used in the GCE model was derived from IFA sounding networks (Lin and Johnson 1996).

Cloud systems (nonsquall clusters, a squall line, and scattered convection) for the period 1–8 September 1974 phase III of GATE have also been simulated using the GCE model (Li et al. 1999; Tao 2003). Sui and Yanai (1986) provided the GATE large-scale forcing for the GCE model. The same large-scale forcing was used in Grabowski et al. (1996). The large-scale environments associated with the organized cloud systems that occurred in TOGA COARE and GATE were quite different even though both are over tropical oceans. The large-scale advective forcing in temperature and water vapor (see Fig. 1), as well as the large-scale vertical velocity, are stronger for TOGA COARE. The vertically integrated water vapor content (precipitable water) is lower for the GATE case compared to the TOGA COARE cases (Table 1). The mean CAPE is slightly smaller in GATE than in TOGA COARE.

For TOGA COARE, compared to the 10–17 December period, the vertical shear of the mean horizontal *u*-wind component in the low troposphere was stronger for the 19–27 December convective episode (Fig. 2). This likely indicates that there will be a greater contribution to heating from stratiform precipitation for the 19–27 December case (Lin and Johnson 1996). The strong surface wind for the 19–27 December period can also generate strong surface fluxes as compared to the very weak surface wind in the SCSMEX cases, which can only produce small surface fluxes (see Table 3 and the discussion in the results section). For the ARM cases, the surface fluxes are prescribed, and the surface wind does not interact with the boundary layer. Please refer to Das et al. (1999) for GATE, Johnson et al. (2002) and Tao et al. (2000) for the TOGA COARE cases, Tao et al. (2003a) for the SCSMEX cases, and Xu et al. (2002) for the ARM cases with regard to the temporal variation of the wind shear.

The South China Sea Monsoon Experiment (SCSMEX) was conducted in May–June 1998, and one of its major objectives is to understand better the key physical processes for the onset and evolution of the summer monsoon over Southeast Asia and southern China (Lau et al. 2000). Two multiday integrations using SCSMEX data (Johnson and Ciesielski 2002) were simulated using the GCE model (Tao et al. 2003a). The first one is prior to and during the monsoon onset period (18–26 May 1998), and the second is after the onset of the monsoon (2–11 June 1998). The mean large-scale forcing associated with these two cases is different (Fig. 1). For example, the large-scale forcing in water vapor is much stronger in the lower and middle troposphere in the June case. In addition, the CAPE is larger in the June period than in the May one (Table 1). Note that the large-scale forcing in water vapor has more complex vertical structures (multiple peaks) compared to the large-scale forcing in temperature (single peaks located at middle altitudes, see Fig. 1). The vertically integrated water vapor contents are very moist for the SCSMEX cases compared to the two TOGA COARE cases.

The ARM summer 1997 Intensive Observing Period (IOP) at the Southern Great Plains (SGP) Cloud and Radiation Testbed (CART) site in northern Oklahoma covers a 29-day period from 18 June to 17 July. Three subperiods, 26–30 June, 7–12 July, and 12–17 July 1997, are simulated using the GCE model.[2] One major difference between the ARM simulations and the SCSMEX, TOGA COARE, and GATE simulations is that interactive cloud–radiation and air–sea processes are not allowed in the ARM runs. Radiative heating rate profiles based on the European Centre for Medium-Range Weather Forecasts (ECMWF) that are adjusted by the observed column radiative fluxes and observed surface turbulent (latent and sensible) heat fluxes from energy balance/Bowen ratio (EBBR) measurements are imposed. As expected, the atmosphere is dryer and more unstable (i.e., has a large CAPE) in these midlatitude, continental ARM cases than those over tropical oceans (Table 1). The large-scale forcing in temperature and water vapor for the ARM cases is also quite different from their tropical, oceanic counterparts (Fig. 1). See Zhang and Lin (1997) and Xie et al. (2001) for more details on the ARM cases and their associated large-scale forcing.

The standard deviation of CAPE and precipitable water associated with these cases is also shown in Table 1. A very large standard deviation is found in CAPE for the ARM cases but not for the tropical, oceanic cases. Also, the standard deviation of CAPE (36% to 92% compared to its mean) is much larger than the standard

[2] These same three periods have been used by the GCSS working group 4 (WG4) model intercomparison project for CRMs and single column models (SCMs).

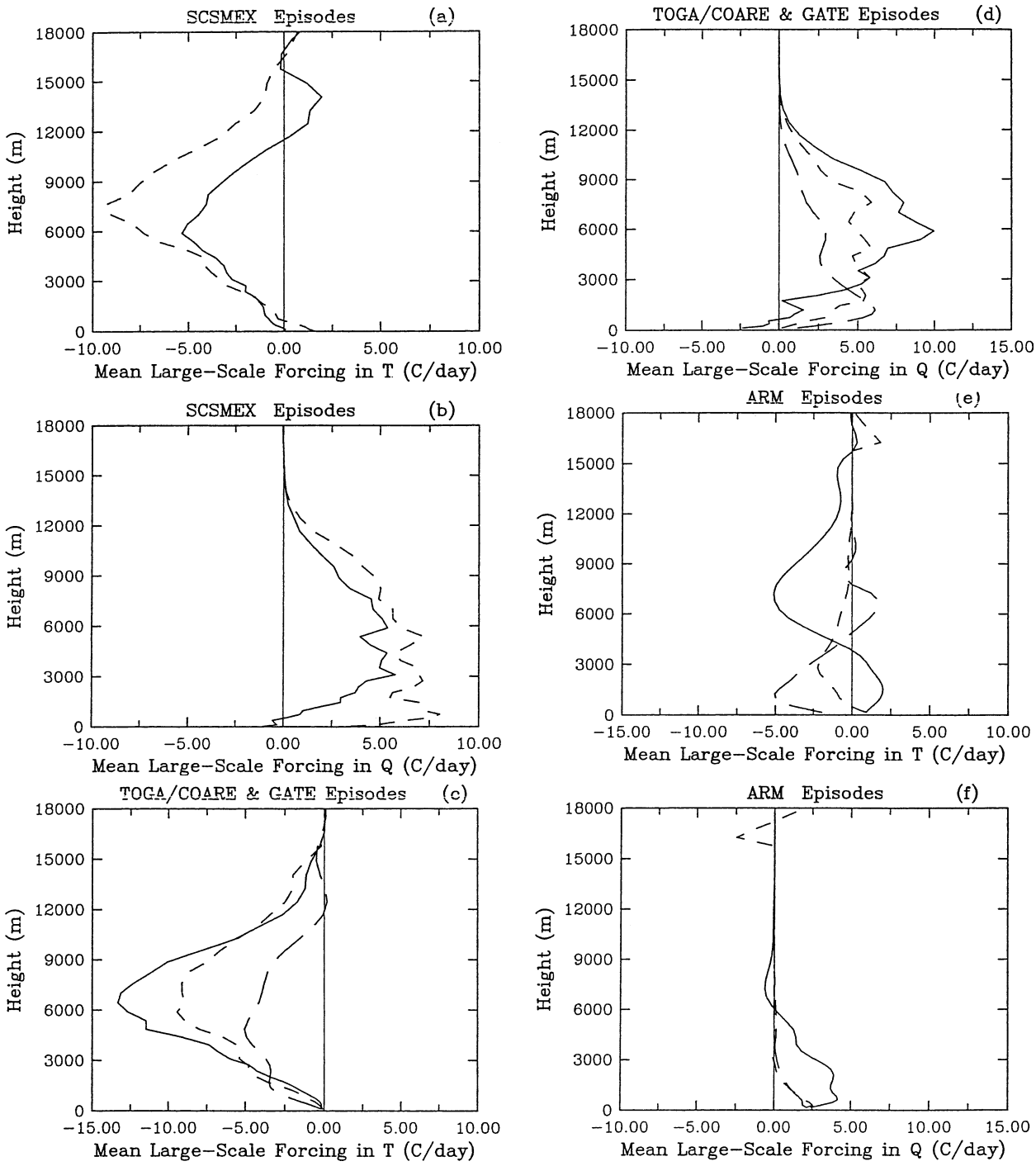

FIG. 1. Time-averaged large-scale advective forcing in (a) temperature and (b) water vapor for the SCSMEX cases (solid line is the 18–26 May 1998 period and the dashed line the 2–11 Jun 1998 period). (c), (d) As in (a) and (b) except for TOGA COARE (solid line is 10–17 Dec and the dashed line 19–27 Dec 1992) and GATE (long-dashed line is 1–8 Sep 1974) cases. (e), (f) As in (a) and (b) except for the three ARM cases (solid line is 26–30 Jun, dashed line 7–12 Jul, and long-dashed line 12–17 Jul 1997).

TABLE 1. Initial environmental conditions expressed in terms of convective available potential energy and precipitable water for the SCSMEX (18–26 May and 2–11 Jun 1998), TOGA COARE (10–17 and 19–27 Dec 1992), GATE (1–8 Sep 1974), and ARM (26–30 Jun, 7–12 Jul, and 12–17 Jul 1997) cases. The standard deviation of CAPE and precipitable water are also shown.

	CAPE (m^2 s^{-2})		Precipitable water (g cm^{-2})	
	Mean	Std dev	Mean	Std dev
SCSMEX 18–26 May 1998	825	499	62.53	1.89
SCSMEX 2–11 Jun 1998	1324	848	62.34	2.94
TOGA 19–27 Dec 1992	898	422	54.64	1.54
TOGA 10–17 Dec 1992	1238	364	56.48	1.95
GATE 1–8 Sep 1974	736	412	47.61	2.98
ARM 26–30 Jun 1997	1954	1044	37.76	3.05
ARM 7–12 Jul 1997	1761	1617	37.56	4.56
ARM 12–17 Jul 1997	2806	1017	36.80	2.37

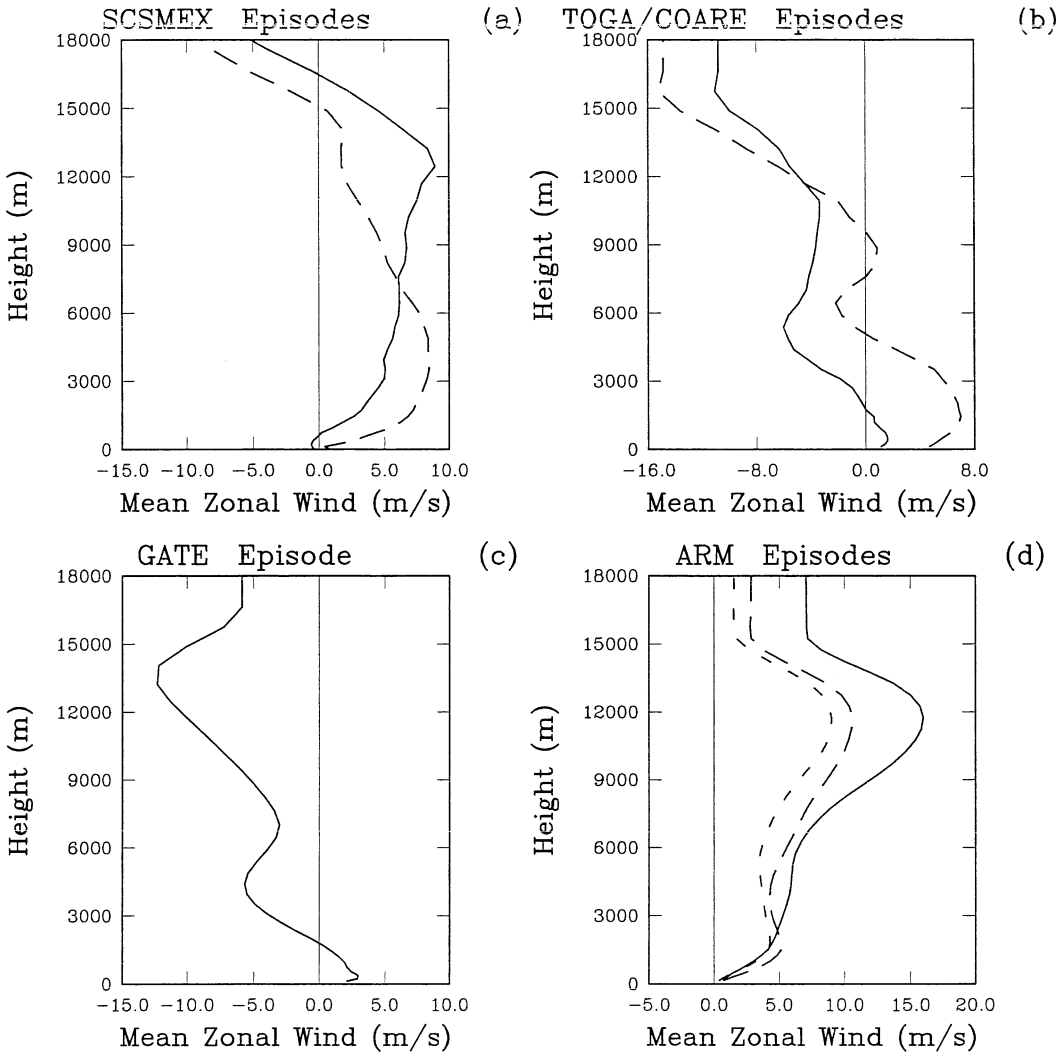

FIG. 2. Time-averaged large-scale (a) *u*-wind for the two SCSMEX cases. The solid line is for the 18–26 May 1998 period and the dashed line is for the 2–11 Jun 1998 period. (b) As in (a) except for TOGA COARE (solid line is 10–17 Dec and dashed line 19–27 Dec 1992) cases. (c) As in (a) except for GATE (1–8 Sep 1974) case. (d) As in (a) except for the three ARM cases (solid line is 26–30 Jun, dashed line 7–12 Jul, and long-dashed line 12–17 Jul 1997).

deviation of precipitable water (less than 12% relative to its mean).

3. The Goddard Cumulus Ensemble model

The model used in this study is the 2D version of the Goddard Cumulus Ensemble (GCE) model. The equations that govern cloud-scale motion (wind) are anelastic by filtering out sound waves. The subgrid-scale turbulence used in the GCE model is based on work by Klemp and Wilhelmson (1978) and modified by Soong and Ogura (1980) by including the effect of condensation on the generation of subgrid-scale kinetic energy. The cloud microphysics include a parameterized two-category liquid water scheme (cloud water and rain), and a parameterized Lin et al. (1983) or Rutledge and Hobbs (1984) three-category ice-phase scheme (cloud ice, snow, and hail/graupel). Graupel is used in the SCSMEX, TOGA COARE, and GATE simulations and hail is used for the ARM cases. Shortwave (solar) and longwave (infrared) radiation parameterizations are also included in the model (Tao et al. 1996). The TOGA COARE bulk flux algorithm (Fairall et al. 1996) is linked to the GCE model for calculating surface fluxes over ocean (Wang et al. 1996). All scalar variables (potential temperature, mixing ratio of water vapor, turbulence coefficients, and all five hydrometeor classes) use forward time differencing and a positive definite advection scheme with a nonoscillatory option (Smolarkiewicz and Grabowski 1990). The dynamic variables, *u, v,* and *w,* use a second-order accurate advection scheme and a leapfrog time integration (kinetic energy semiconserving method). Details of the GCE model description and improvements can be found in Tao and Simpson (1993) and Tao et al. (2003b).

For the present study, a stretched vertical coordinate with 41 levels is used. The model has finer resolution (about 80 m) in the boundary layer and coarser resolution (about 1000 m) in the upper levels. The grid spacing in the horizontal plane is 1000 m with 512 grid points. The time step is 6 s for the ARM cases and 7.5 s for the SCSMEX, TOGA COARE, and GATE cases.

4. Results

a. Atmospheric thermodynamic energy budget

Horizontal and vertical integration of the equations for temperature, water vapor (q_v), and moist static energy h ($h = C_pT + L_vq_v + gz$) over the entire model domain yields

$$C_p\left\langle\frac{\partial\overline{T}}{\partial t}\right\rangle = \langle L_v(\overline{c} - \overline{e}) + L_f(\overline{f} - \overline{m}) + L_s(\overline{d} - \overline{s})\rangle - C_p\left\langle\frac{\partial\overline{T}}{\partial t}\right\rangle_{\text{L.S}} + \overline{Q}_R + C_p\overline{H}_s, \quad (1)$$

$$L_v\left\langle\frac{\partial\overline{q}_v}{\partial t}\right\rangle = -L_v\langle(\overline{c} - \overline{e}) + (\overline{d} - \overline{s})\rangle - L_v\left\langle\frac{\partial\overline{q}}{\partial t}\right\rangle_{\text{L.S}} + L_v\overline{E}_o, \quad \text{and} \quad (2)$$

$$\left\langle\frac{\partial\overline{h}}{\partial t}\right\rangle = \langle L_f(\overline{f} - \overline{m}) + (L_s - L_v)(\overline{d} - \overline{s})\rangle - \left(C_p\left\langle\frac{\partial\overline{T}}{\partial t}\right\rangle_{\text{L.S}} + L_v\left\langle\frac{\partial\overline{q}_v}{\partial t}\right\rangle_{\text{L.S}}\right) + \overline{Q}_R + C_p\overline{H}_s + L_v\overline{E}_o, \quad (3)$$

where $-\langle\partial\overline{T}/\partial t\rangle_{\text{L.S}}$ and $-\langle\partial\overline{q}_v/\partial t\rangle_{\text{L.S}}$ are the large-scale advective cooling and moistening; L_vE_o and C_pH_s are the latent and sensible heat fluxes from the ocean surface; C_p is the specific heat of dry air at constant pressure. The variables L_v, L_f, and L_s are the latent heats of condensation, fusion, and sublimation, respectively. The variables *c, e, f, m, d,* and *s* stand for the rates of condensation, evaporation of cloud droplets and raindrops, freezing of raindrops, melting of snow and graupel, deposition of ice particles, and sublimation of ice particles, respectively. The term Q_R is the cooling/heating rate associated with long- and shortwave radiative processes. The physical processes responsible for the precipitation processes in each case can be quantified by examining the budget. In addition, the similarities and differences in terms of large-scale forcing, surface fluxes, and radiation upon precipitation (net condensation) between different active convective events that developed in different geographic locations can be identified.

Tables 2 and 3 list the temperature and water vapor budgets for the SCSMEX, TOGA COARE, GATE, and ARM cases. In the tropical, oceanic cases (SCSMEX, TOGA COARE, and GATE), the largest two terms in the temperature and water vapor budget are net condensation (heating/drying) and imposed large-scale forcing (cooling/moistening). These two terms are opposite in sign, however. Soong and Tao (1980) performed experiments with different magnitudes of large-scale forcing and found that the larger the large-scale forcing (cooling/moistening), the larger the net condensation (heating/drying). They suggested that the effect of cloud microphysics is simply a response to the *imposed large-scale forcing in temperature and water vapor.* The sensible heat flux is at least one order of magnitude smaller than net condensation and large-scale forcing in these tropical oceanic cases.

The contributions by net radiation (shortwave heating and longwave cooling) and latent heat flux on the net condensation vary in these tropical cases, however. For the SCSMEX and GATE cases, the net radiation (cooling) accounts for about 20% or more of the net condensation. This result suggests that net radiation plays an important role in the precipitation processes for the

TABLE 2. Temperature budgets for the SCSMEX, TOGA COARE, GATE, and ARM cases. Net condensation is the sum of condensation, deposition, evaporation, sublimation, freezing, and melting of cloud. Large-scale forcing is the imposed large-scale advective effect on temperature, and $d(T)$ is the local time change of temperature. Longwave cooling, shortwave heating, and their net radiative processes are shown in Q_R. Units are in °C day^{-1}.

	dT/dt	Net condensation	Large-scale forcing	Net Q_R = SW − LW	Sensible heat fluxes
SCSMEX (18–26 May 1998)	−0.12	2.83	−2.03	−0.95	0.03
SCSMEX (2–11 Jun 1998)	0.26	4.17	−2.88	−1.04	0.01
TOGA COARE (19–27 Dec 1992)	−0.29	5.06	−5.55	0.03	0.17
TOGA COARE (10–17 Dec 1992)	−0.28	4.33	−4.61	−0.11	0.11
GATE (1–8 Sep 1974)	−0.20	3.13	−2.67	−0.68	0.02
ARM (26–30 Jun 1997)	0.83	2.16	−1.01	−0.63	0.31
ARM (7–12 Jul 1997)	0.67	1.37	−0.41	−0.51	0.22
ARM (12–17 Jul 1997)	−0.16	1.28	−1.05	−0.66	0.27

SCSMEX and GATE cases through increased or reduced relative humidity (i.e., Tao et al. 1996; Sui et al. 1998). Net radiation is very small and does not contribute to the temperature budget for the TOGA COARE cases (Table 2). Figure 3 shows the time- and domain-averaged total, shortwave heating and longwave cooling profiles for one of the TOGA COARE cases and one of the SCSMEX cases. For the TOGA COARE case, there is strong radiative cooling at and near the tropopause and heating below, but this radiative cooling and heating canceled each other in the net atmospheric radiation budget. The radiative heating and cooling are mainly caused by the larger stratiform and anvil clouds simulated in the TOGA COARE cases compared to the others (see the SCSMEX case shown in Fig. 3). However, the radiation process still plays an important role in the diurnal variability of rainfall for the TOGA COARE convective systems (Sui et al. 1998; Johnson et al. 2002; and others). A detailed review on cloud–radiation interaction using CRMs and mesoscale models was shown in Tao (2003). Radiation can play an important role in the temperature budget and on precipitation processes through increased or reduced relative humidity (Tao et al. 1996; Sui et al. 1998).

Surface moisture fluxes are not negligible in the water budget in the tropical convective systems except for one of the SCSMEX cases. Surface moisture flux is an order of magnitude smaller than both large-scale forcing and net condensation in the water vapor budget for the June SCSMEX case. This is because the large-scale advective forcing in water vapor was very large in the lower troposphere and generated a moist boundary layer (Fig. 1). The very weak surface wind in the SCSMEX cases (Fig. 2) could also contribute to small latent heat fluxes. In addition, the mean sea surface temperature (SST) is about 28°C, and the difference in air and SST is small for the SCSMEX cases. This could also explain the small latent heat fluxes in the SCSMEX cases. This reduced the contribution from latent heat fluxes from the ocean for this case. There are direct and indirect observations of surface evaporation showing about 1.7 and 1.03 mm h^{-1} for the SCSMEX May and June cases, respectively (Johnson and Ciesielski 2002). These are larger than those simulated by the GCE model. The modeled surface relative humidity is about 5% higher than observed (sounding). This could explain the smaller latent heat fluxes simulated by the model. Based on budget calculations, these differences could improve the simulated rain amount by 4% and 2%, respectively, for the May and June cases. This difference, however, is still too small to explain the difference between the modeled and sounding-estimated rainfall (shown in Table 5).

Net radiation and sensible and latent heat fluxes play a much more important role in the three ARM cases than in the tropical cases (Tables 2 and 3). Latent heat fluxes are much larger than the large-scale forcing in the water vapor budget for the two July cases (relatively

TABLE 3. As in Table 2 except for the water budgets. Net condensation is the sum of condensation, deposition, evaporation, and sublimation of cloud. Large-scale forcing is the imposed large-scale advective effect on water vapor, and $d(q_v)$ is the local time change of water vapor. Units are in mm day^{-1}.

	$d(Q_v)/dt$	Net condensation	Large-scale forcing	Latent heat fluxes
SCSMEX (8–26 May 1998)	−0.15	−11.23	9.81	1.27
SCSMEX (2–11 Jun 1998)	1.12	−16.45	16.84	0.73
TOGA COARE (19–27 Dec 1992)	0.57	−20.15	15.03	5.69
TOGA COARE (10–17 Dec 1992)	−0.80	−17.31	13.47	3.04
GATE (1–8 Sep 1974)	−0.33	−12.30	9.90	2.07
ARM (26–30 Jun 1997)	1.24	−8.13	5.29	4.08
ARM (7–12 Jul 1997)	−0.02	−5.07	1.19	3.86
ARM (12–17 Jul 1997)	0.31	−4.83	0.80	4.34

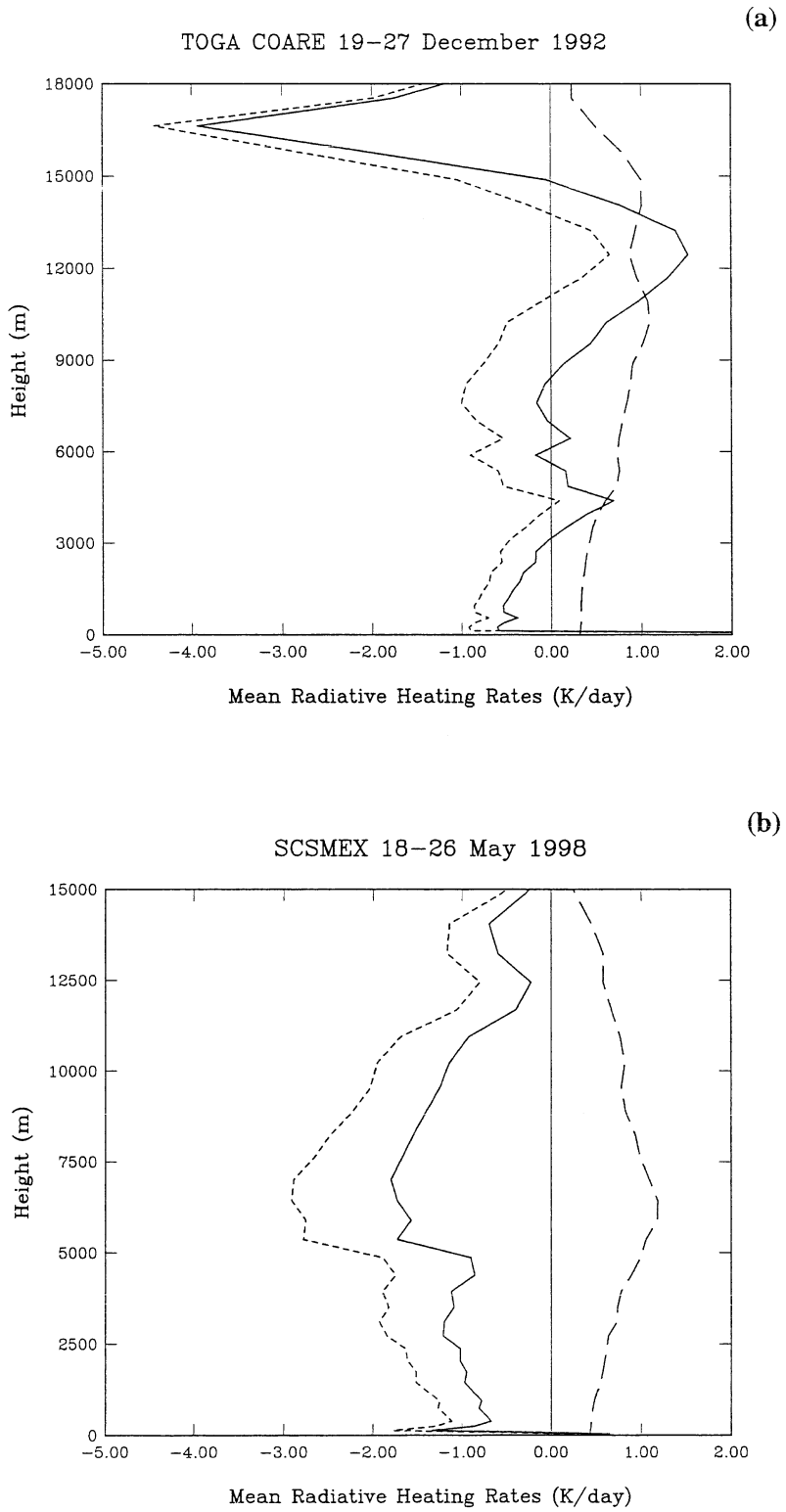

FIG. 3. Time-averaged total heating/cooling, longwave cooling, and shortwave heating for (a) one of the TOGA COARE (19–27 Dec 1992) and (b) one of the SCSMEX (18–26 May 1998) cases. The solid line is for total radiation, long-dashed line for shortwave heating, and short-dashed line for longwave cooling.

weak events compared to the other cases). They balance 76% and 90% of the net condensation for the two July cases, respectively. They are the main source of moisture for condensation. Net radiation can be as large as the large-scale temperature forcing in the ARM cases (Table 2). This means the accurate measurement of surface fluxes and radiation is crucial for simulating the ARM cases.

It is known that temperature and water vapor are closely related. Evaporative cooling/condensational heating is a source/sink for the water vapor field. On the other hand, latent heat flux from the ocean surface can provide water vapor for condensation heating. The moist static energy budget (Table 4) can provide some additional information on the physical processes for these active convective events. The net condensation terms in the moist static energy budget are net freezing [freezing (heating) minus melting (cooling)], and the product of the latent heat of fusion and the net deposition [deposition (heating) minus sublimation (cooling)]. These microphysical processes are usually the smallest terms in the moist static energy budget.

Large-scale forcing and surface latent heat fluxes are largest in the TOGA COARE cases. They are approximately an order of magnitude larger than the other processes in the moist static energy budget. Interestingly, the large-scale forcing in the moist static energy budget is negative as a result of a larger absolute value of large-scale advection of sensible heat (cooling) compared to large-scale advection of latent heat (moistening) for the TOGA COARE and GATE cases. For SCSMEX, however, there is more large-scale moistening than cooling. This suggests that the imposed large-scale advective forcing in water vapor is important for convective processes in the SCSMEX cases. The net radiation is quite important in the SCSMEX, GATE, and ARM cases. For some cases, it is the largest term in the moist static energy budget.

Note that the net condensation is very small in both the TOGA COARE cases and in two of the ARM cases. This suggests that there is a balance between the melting and freezing, and the deposition and sublimation in these cases. A positive (negative) value in net condensation in the moist static energy indicates the sum of freezing and deposition is larger (smaller) than the sum of melting and sublimation.

The surface (sensible and latent heat) fluxes are largest in the ARM cases. However, the surface budget for the June ARM case is different from the two July cases. First, the large-scale water vapor forcing is important and contributes about 65% of the net condensation in the June case (Table 3). Second, the large-scale water vapor forcing is stronger than the large-scale temperature forcing in the June case (Table 4).

The tendency (local change) term is very small compared to net condensation, large-scale forcing, and latent heat fluxes in the temperature and water vapor budgets (Tables 2 and 3). But, it is comparable with other terms

TABLE 4. As in Table 3 except for the moist static energy budget. Units are W m^{-2}. Note that a 1°C day^{-1} cooling or warming in the local change term over the whole troposphere can lead to about 92 W m^{-2} in the temperature budget. Note that 1 g kg^{-1} in the local time change over the whole troposphere can lead to about 280 W m^{-2} in the water vapor budget.

					Heat fluxes	
	$D(C_pT + L_vQ_v)/Dt$	Net condensation	Large-scale forcing	Net Q_R	Sensible	Latent
SCSMEX	−18.0	2.84	48.8	−110.7	4.2	36.85
SCSMEX	62.4	3.55	156.6	−119.9	1.07	21.11
TOGA COARE	−16.71	0.49	−204.96	3.34	19.76	164.66
TOGA COARE	−55.15	−0.98	−142.57	−12.75	13.24	87.91
GATE	−32.27	4.48	−21.14	−77.69	2.35	59.73
ARM	126.35	0.75	42.91	−68.93	33.62	118.00
ARM	72.24	2.14	−10.54	−54.96	23.85	111.75
ARM	−8.27	−0.78	−90.75	−72.19	29.74	125.71

TABLE 5. Precipitation efficiencies (%), domain-averaged surface rainfall amounts (mm day^{-1}), and total positive cloud condensation (condensation plus deposition, in mm day^{-1}) for the SCSMEX, TOGA COARE, GATE, and ARM cases. Rainfall estimated by sounding network is also shown. Please see text for definition of the two different PEs.

	Precipitation efficiency		Rainfall (mm day^{-1})		Total condensation (mm day^{-1})
	(PE_1)	(PE_2)	Modeled	Observed	
SCSMEX (18–26 May 1998)	45.4	31.2	11.14	13.00	24.56
SCSMEX (2–11 Jun 1998)	45.3	31.2	16.46	20.71	36.31
TOGA COARE (19–27 Dec 1992)	41.6	29.4	20.15	20.10	48.39
TOGA COARE (10–17 Dec 1992)	37.5	27.3	17.81	17.78	47.52
GATE (1–8 Sep 1974)	44.5	30.8	12.31	13.54	27.67
ARM (26–30 Jun 1997)	40.1	28.6	7.51	8.21	18.72
ARM (7–12 Jul 1997)	39.9	28.5	4.68	4.17	11.74
ARM (12–17 Jul 1997)	32.1	24.3	4.29	4.22	13.37

in the moist static energy budget. A 1°C day^{-1} cooling or warming and 1 g kg^{-1} in the local change term over the whole troposphere, respectively, can lead to about 92 W m^{-2} in the temperature budget and about 280 W m^{-2} in the water vapor budget.

b. Large-scale precipitation efficiency

The definition of the PE varies in different observation and modeling studies. It generally includes total rainfall measured or simulated at the ground, the total water vapor flux into the storm, and microphysics (i.e., net condensation). In observational studies, the PE is typically defined as the ratio between total surface rainfall and the total inflow of water vapor into the storm through cloud base. In a numerical modeling study, Weisman and Klemp (1982) equated the total moisture influx into a storm with the total condensation within the modeled storm. In an another modeling study, Lipps and Helmer (1986) defined the PE (or cloud efficiency) as the ratio of the total rainfall to the positive cloud condensation (condensation onto water plus deposition onto ice). Ferrier et al. (1996) investigated the different definitions of PE using the 2D version of the GCE model with sophisticated ice microphysics. In this modeling study, two different PEs are estimated. The first one is defined as the ratio of the total rainfall to the total positive cloud condensation

$$\mathrm{PE}_1 = \frac{R}{C_{\mathrm{cd}}}, \tag{4}$$

where C_{cd} is the sum of condensation plus deposition. This definition is the same as Weisman and Klemp (1982) and Lipps and Helmer (1986) except that no ice processes were used in Weisman and Klemp (1982) and Lipps and Helmer (1986). The second is defined as the ratio of total rainfall to the sum of total net condensation and total rainfall,

$$\mathrm{PE}_2 = \frac{R}{R + C_{\mathrm{cd}}}. \tag{5}$$

In this definition, PE_2 varies between 0 and 1. When the total condensation is very small, the PE will be 1. This could happen if some of the ensemble of clouds/cloud systems are in the decaying stage. The PE will be 0 when there is no surface rainfall (i.e., during the developing stage of clouds/cloud systems). The other definitions could allow the PE to be greater than one.

1) GCE MODEL RESULTS

The total PE_2 ranges from 24% to 31% in the GCE-simulated SCSMEX, TOGA COARE, GATE, and ARM cases (Table 5). The two SCSMEX cases have identical PE_2 (31.2%) and are the largest among all the simulations. This result suggests that the larger vertical *u*-wind shear at low and middle troposphere in the June SCSMEX case does not produce a smaller PE (Fig. 2). However, one of the TOGA COARE cases (19–27 December) has a slightly larger PE_2 and a stronger low-level wind shear than the other TOGA COARE case (10–17 December). It may be expected that the ARM (midlatitude, continental) and GATE cases would have lower PE_2s because they developed under drier environments. One of the ARM July cases has the smallest PE_2 (24.3%), but the GATE and the other two ARM cases have relatively large PE_2 (from 28.5% to 30.8%).

The total PE_1 ranges from 32% to 45% in the GCE-simulated SCSMEX, TOGA COARE, GATE, and ARM cases (Table 5). As expected (by definition), PE_1 is larger than PE_2. Larger PE_1 is always associated with larger PE_2. For example, the two SCSMEX cases and GATE have the largest PE_1, but one of the ARM case (12–17 June) cases has the smallest PE_1. One interesting feature is that the range of PE_2 is smaller than that of PE_1 in these cases.

The precipitation efficiency PE_1 reaches 100% (99% to 103%) for all tropical oceanic cases (SCSMEX, TOGA COARE, and GATE) and about 90% (89% to 92%) for midlatitude continental (ARM) cases if the total positive cloud condensation is replaced by the net condensation (condensation plus deposition minus evaporation and sublimation) in Eq. (4). The balance of the vertically integrated total water vapor in the modeled water budget causes the PE to be near 1 (see Table 3). The drier environment and smaller large-scale advective

forcing in water vapor are the main reasons for the smaller PE_1 in the ARM cases compared to the other cases.

Observed (determined from sounding networks) rainfall is also shown in Table 5 for comparison. The rainfall amount simulated by the GCE model and estimated by soundings is in excellent agreement (within 0.5%) with each other for both TOGA COARE cases (i.e., Johnson et al. 2002). The model underestimates the rainfall by 10%, 17%, and 20%, respectively, for the GATE and SCSMEX May and June cases compared to that calculated based on soundings (Das et al. 1999; Tao et al. 2003a). For the ARM cases, however, the GCE model underestimates rainfall by about 8.5% in the June case and overestimates rainfall by 12% and 2%, respectively, for the two July cases (Xu et al. 2002).[3] All of these cases are forced by a prescribed large-scale advective forcing determined from soundings. The radiation and surface fluxes can be influenced by clouds simulated by the models and may cause the rainfall differences between the model and the sounding estimates. For the ARM cases, the radiation and surface fluxes are prescribed, but not for the SCSMEX, GATE, and TOGA COARE cases. The model physics may be another reason for this discrepancy. Accurate and consistent large-scale advective tendencies in temperature and water vapor are also needed for CRM simulation. Tao et al. (2000) found that the large-scale advective terms for temperature and water vapor are not always consistent. For example, large-scale forcing could indicate strong drying (which would produce cooling in the model through evaporation) but not contain large-scale advective heating to compensate. This discrepancy in forcing would cause differences between the observed and modeled rainfall.

Based on the moist static energy budget (Table 4), the GCE can underestimate the rainfall when a positive large-scale forcing is imposed/prescribed (except for the GATE case). This result may imply that the GCE model could underestimate the rainfall (when compared to sounding estimates) when the large-scale advective water vapor forcing exceeds the large-scale temperature forcing. Only eight cases are simulated in this modeling study. More cloud ensemble modeling studies will be needed to generalize this relationship as well as the relationship between PE and net condensation in the moist static energy budget. The error (or difference) between the model and sounding estimates can affect the magnitude of the simulated PE (a few percent increase in the SCSMEX, GATE, and one of the ARM cases, but decrease in another ARM case). However, the error (difference) cannot change the major conclusions of the paper (i.e., high PE in the SCSMEX and GATE cases and low PE for one of the ARM cases).

Generally, the model results show that there is no clear relationship between the two PEs and rainfall, the total positive condensation, or the large-scale forcing. However, the model results show that the two SCSMEX cases and the GATE case have large, positive net condensation terms in the moist static energy budget, and they all have larger PEs. One of the ARM June cases and one of the TOGA COARE cases have negative net condensation terms as well as small PEs. A positive net condensation term in the moist static energy budget indicates that there is net freezing (freezing minus melting) and/or net deposition (deposition minus sublimation).

2) Previous modeling studies and one recent observational study

Weisman and Klemp (1982) investigated the PE associated with midlatitude, deep, moist convection and its sensitivity to wind shear and buoyancy. Their results showed that PEs varied from 11% to 49% over the 2-h duration of their three-dimensional (3D) model simulations. The PEs decrease with increasing wind shear at low buoyancies and low to moderate shear regimes. Their results also showed that the PE can increase with wind shear and buoyancy in associating with the development of split storms (with strong shear and very strong convective updrafts). In a 3D model simulation of deep, tropical convection Lipps and Helmer (1986) indicated that PE was approximately 40% over the 4-h integration. Their result is comparable to the cases with weak or no wind shear in Weisman and Klemp (1982).

Ferrier et al. (1996) used the 2D GCE model (952-km-wide domain and 6-h integration[4]) to investigate the factors responsible for PEs in midlatitude and tropical squall systems. Their results indicated that the vertical orientation of the updrafts and the ambient moisture content are the major factors that determine the PE of a storm. Vertically erect updrafts promote the most effective collection of cloud condensate by rapidly falling precipitation species. Ferrier et al. (1996) found that downshear tilted convection is also quite efficient because the gust fronts are too weak to block all of the low-level inflow, causing some of the ambient air to pass through the cold pool without being carried up into deep updrafts (i.e., PE of 0.45 for a midlatitude squall system). However, upshear sloping convection possesses deeper and broader areas of subsaturation in the stratiform region, the evaporative loss of rain is greater than in downshear tilted and erect storms. The increasing contribution of stratiform precipitation to total rainfall as the systems slanted more in the upshear direction is consistent with their being less efficient (i.e., PE of

[3] Similar errors have been found with other CRMs in simulating ARM and TOGA COARE cases.

[4] In Ferrier et al. (1996), the GCE model domain consisted of 612 grid points with a constant grid spacing of 1000 m in the innermost 512 grid points embedded within a stretched region. This outer stretched region made the model less sensitive to the choice of gravity wave speed associated with open lateral boundary conditions.

0.24). The organization of cloud/cloud system is mainly determined by the vertical shear of the horizontal wind. Ferrier et al. (1996) also indicated that PE is higher in moist versus drier environments as a result of larger condensation rates, whereas variations in cloud and rain evaporation rates are much smaller. Since the ambient moisture affects storm condensation through the vertical advection of water vapor, the development and intensity of convection is strongly modulated by the height and depth of dry layers above the boundary layer. Furthermore, the degree of modulation is expected to increase for environments with weaker thermodynamic instability.

Lucas et al. (2000) also used the 2D version of the GCE model to examine the PE associated with tropical squall lines and their sensitivity to tropospheric wind and moisture profiles. The PE was based on 4-h averages (from hours 2 to 6) of simulated systems. Their results indicated that increased midlevel shear (simulated system becomes upshear tilted) results in a lower PE and a higher fraction of stratiform rain. As humidity is increased, model systems transition from weak, unsteady systems with little precipitation to strong, upshear titled systems with increased rainfall and PE (ranges from 0.16 to 0.36).

Shepherd et al. (2001) used the 2D version of ARPS (Advanced Regional Prediction System) to study the rainfall morphology in Florida convergence zones. The warm rain and ice microphysics in the ARPS is based on one of the microphysics schemes in the GCE model (Tao and Simpson 1993; Tao et al. 2003b). The simulated PE ranges from 0.31 to 0.44 for isolated clouds over 1.5 hours of integration. Their results also show that larger PEs are associated with moister environments. These results from Lucas et al. (2000) and Shepherd et al. (2001) are consistent with those obtained from Ferrier et al. (1996).

Shie et al. (2003) examined the PE associated with different quasi-equilibrium states in the Tropics simulated by the 2D version of the GCE model. Their results showed that PEs ranged from 50% to 53% for upright convective clouds that developed in the presence of weak wind shear, and from 41% to 42% for well-organized, tilted stratiform clouds that developed in the presence of strong wind shear. Their results are also consistent with those obtained from Ferrier et al. (1996).

Oury et al. (2000) estimated a PE of 0.31 for a TOGA COARE mesoscale convective system (MCS) using dual-beam airborne radar. It was based on an instantaneous observation over about a 60 km $\times$ 40 km domain. This PE estimate is sensitive to the *Z–R* relationship and sampling area. Chong and Hauser (1989) estimated a PE of about 0.50 for a tropical squall line observed over land in West Africa. The squall line observed in Chong and Hauser was more mature and stationary. It had a full-grown stratiform region (over 200 km).

3) Comparison with previous studies

Precipitation efficiency estimated from previous model studies was mainly associated with an isolated cloud/cloud system and for a 2–6-h time integration. Here PE_2 and its relationship with relative humidity and the vertical shear of the horizontal wind are also examined using 6-hourly model data.[5] Figure 4 shows PE_2 versus the domain-averaged mass-weighted relative humidity. In general, the TOGA COARE and SCSMEX environments are very moist (relative humilities 60%–70%), the ARM environment fairly dry (40%–50%), and GATE is moderately moist (58%). Correspondingly, PE_2 tends to be high in SCSMEX, TOGA COARE, and GATE. This result, PE being higher in moister environments, is in good agreement with those from Ferrier et al. (1996) and Shepherd et al. (2001). However, individual (6-hourly) PE_2 can be over 40% for the ARM cases or very small (less than 10%) for the SCSMEX and TOGA COARE cases. These results suggest that individual PE may not necessarily be higher in moister environments. The results also suggest that the PE_2 increases slightly with mass-weighted relative humidity for one of the SCSMEX cases (18–26 May), one of the TOGA COARE cases (19–27 December), and two of the ARM cases (26–30 June and 7–12 July). One of the ARM cases (12–17 July) has a negative relation. Note that this ARM case has the largest CAPE (Table 1) and weakest (or smallest) large-scale forcing in water vapor (Table 3). The relationship between PE and relative humidity is not very significant, however. For example, an increase of mass-weighted relative humidity by a few percent, can increase the PE_2 from less than 10% to 40%. The results also show that the standard deviation of PE_2 from its mean is smaller than its counterpart in mass-weighted relative humidity.

The impact of middle and upper tropospheric moisture on the PE is also examined (Fig. 5). Again the TOGA COARE and SCSMEX environments are relatively moist (40%–50%), with PE_2 for these cases also being relatively high. Meanwhile, two of the ARM cases are in a very dry environment (20% or less) with PE_2 for these cases being low. This result is in good agreement with Lucas et al. (2000). The model results, however, suggest that the relationship between PE_2 and middle and upper tropospheric moisture is not significant for these cases.

Figure 6 shows PE_2 versus low-level (surface to 700 mb) wind shear. The wind shear associated with these cases is relatively low to moderate. It appears that high (low) PE can occur in low (moderate) shear regimes or vice versa. The lines shown in Fig. 6 are the least square polynomial fits relating PE to wind shear. The results clearly indicate that there is no strong correlation be-

[5] The PE_1 and PE_2 have a very similar relationship with mass-weighted relative humidity and the vertical shear of horizontal wind (shown in Figs. 4–7).

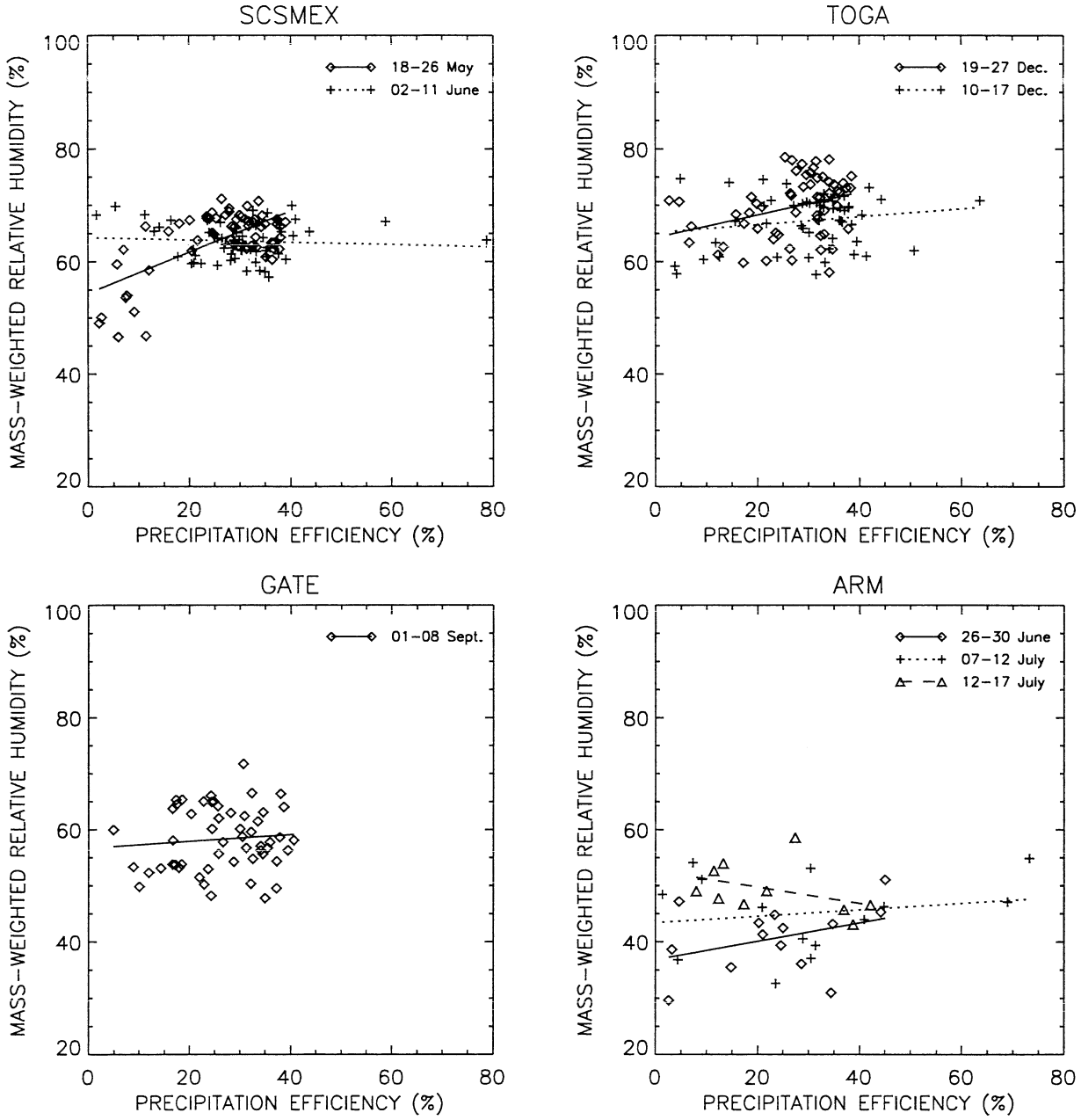

FIG. 4. Precipitation efficiency (%) vs the mass-weighted relative humidity from the surface to the top of the model domain. The lines show the least square polynomial fits. Results are 6-hourly model data for (a) SCSMEX, (b) TOGA COARE, (c) GATE, and (d) ARM.

tween PE_2 and wind shear for the two SCSMEX cases and two of the ARM cases. For one of the TOGA COARE (19–27 December) and one of the ARM (26–30 June) cases, PE_2 decreases with increasing wind shear. For these cases, a decrease in PE with increasing wind shear in low to moderate shear regimes is in agreement with Weisman and Klemp (1982) and Shie et al. (2003). Note that these cases have more positive cloud condensation (convective activity) compared to other cases in the same respective geographic regime (Tables 2 and 3). Also note that the correlation (based on the best polynomial fit) are quite weak. On the other hand, PE_2 increases with increasing wind shear in the GATE case and the other TOGA COARE case (10–17 December). Figure 7 shows PE_2 versus middle tropospheric (700 to 400 mb) wind shear. The increase in midlevel wind shear resulting in a lower PE for the TOGA COARE and GATE cases is in good agreement with Lucas et al. (2000). On the other hand, PE_2 increases only slightly with increasing wind shear for the SCSMEX cases.

Since the model allows more than one cloud or cloud

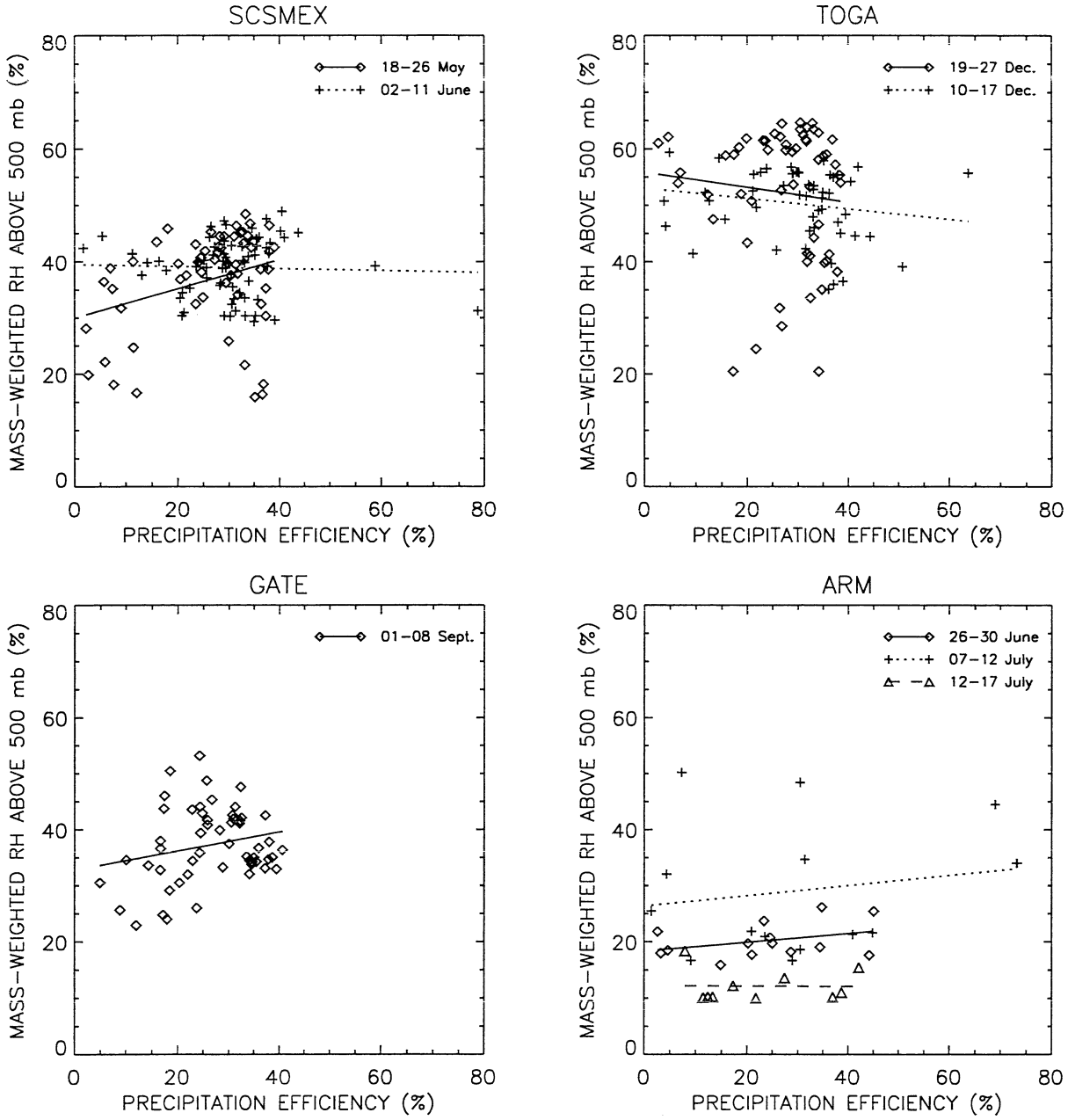

FIG. 5. As in Fig. 4 except for the mass-weighted relative humidity from 500 mb to top of the model domain.

system to develop, cloud–cloud interactions and merging can alter the relationship between cloud organization and wind shear as shown in Moncrieff (1981) and Tao and Simpson (1984). This could be the main reason for a weak or no clear, definite relationship between PE and low or middle tropospheric wind shear. In addition, the large-scale advective forcing imposed in the model might also influence the relationship between PE and mass-weighted relative humidity.

5. Summary and conclusions

The 2D version of the GCE model has been used to simulate two SCSMEX (18–26 May and 2–11 June 1998), two TOGA COARE (10–17 and 19–26 December 1992), one GATE (1–7 September 1974), and three ARM convective active periods (26–30 June, 7–12 July, and 12–17 July 1997) for comparison with each other. Observed large-scale advective tendencies (or forcing) of potential temperature, water vapor mixing ratio, and

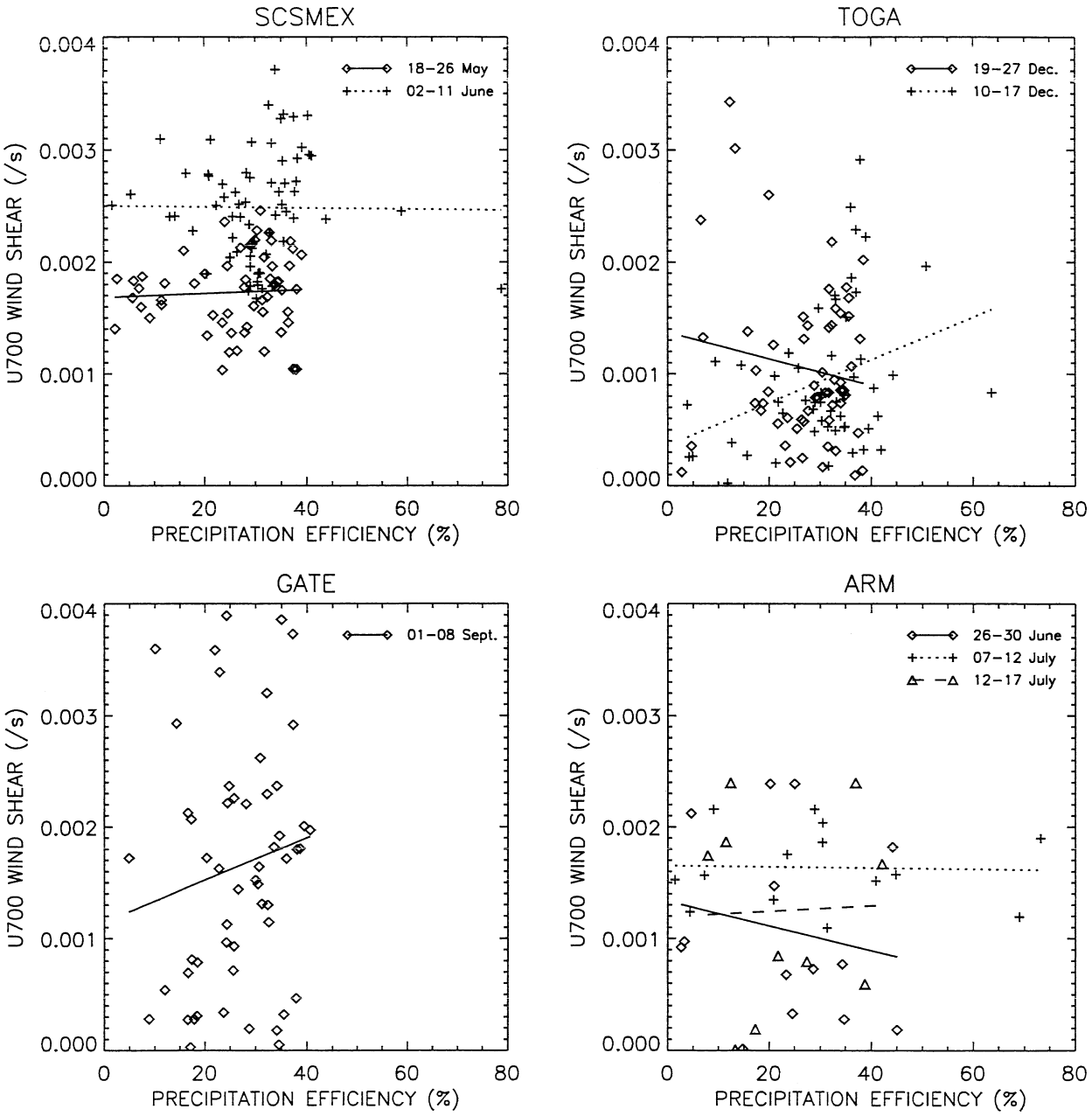

FIG. 6. Precipitation efficiency (%) vs the vertical shear of the horizontal wind (u component) from the surface to 700 mb. Results are 6-hourly model data for (a) SCSMEX, (b) TOGA COARE, (c) GATE, and (d) ARM. Note that a wind shear of 0.001 s^{-1} corresponds to about 3 m s^{-1} between the surface and 700-mb level.

horizontal momentum (Sui and Yanai 1986; Lin and Johnson 1996; Zhang and Lin 1997; Johnson and Ciesielski 2002) are used as the main forcing in governing the GCE model in a semiprognostic manner (Soong and Tao 1980; Tao and Soong 1986; and many others). The atmospheric thermodynamic energy budget and precipitation efficiency were examined by using the model results.

The major results can be summarized as follows.

- Large-scale advective forcing in temperature and water vapor are the major energy sources for net condensation in the tropical, oceanic cases. The large-scale advection of moist static energy is negative, as a result of a larger absolute value of large-scale advection of sensitive heat (cooling) compared to large-scale latent heat (moistening) advection for the TOGA COARE and GATE cases. For SCSMEX, however, there is more large-scale moistening than cooling. In-

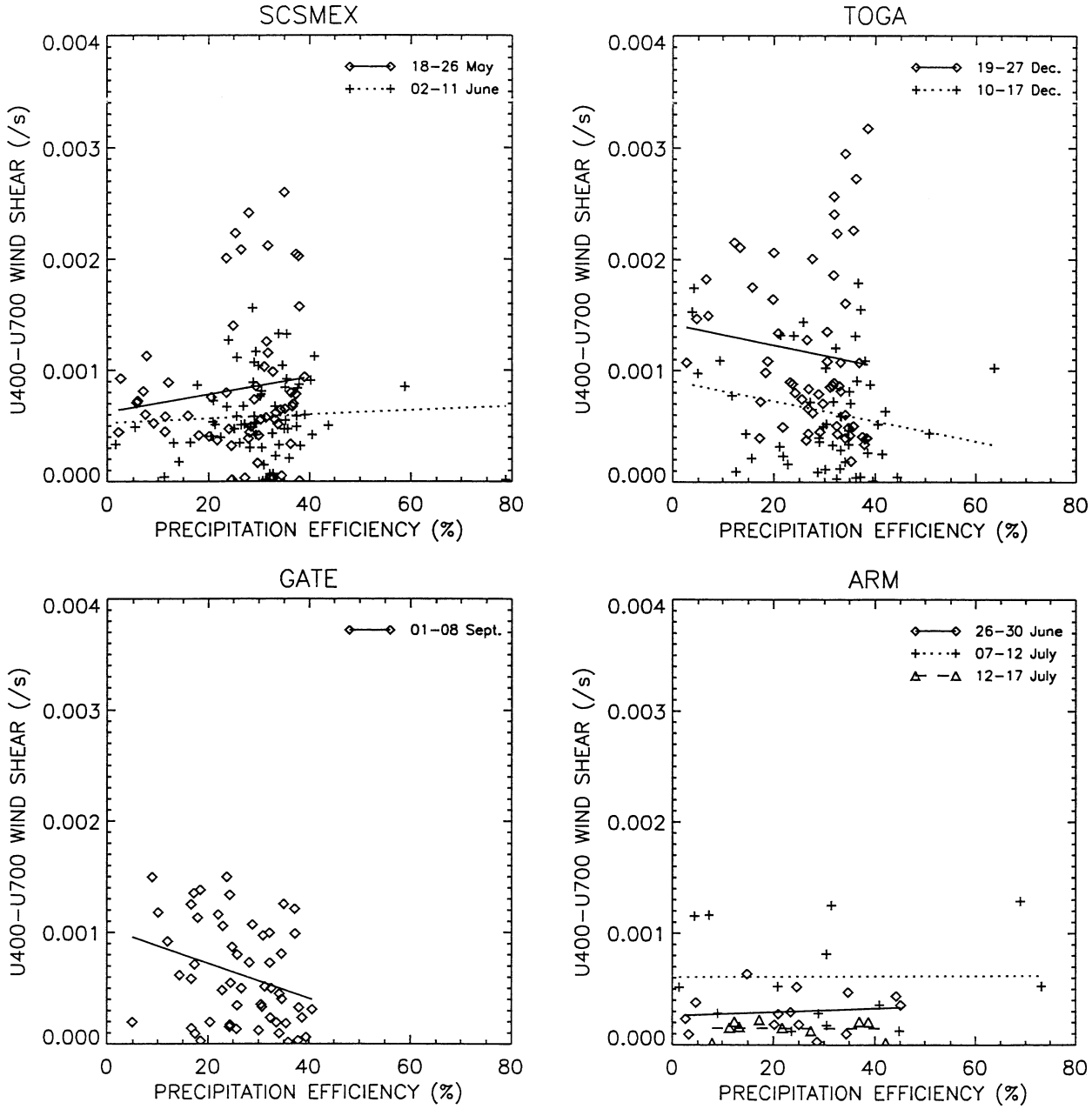

FIG. 7. As in Fig. 6 except for vertical shear of the horizontal wind (u component) from 700 to 400 mb.

terestingly, the vertically integrated water vapor contents are higher for the SCSMEX cases compared to the TOGA COARE and GATE cases.

- The net radiation and the sensible and latent heat fluxes have a much more important role in the energy budget for the three ARM cases. Latent heat fluxes contribute 76% and 90% of the net condensation for the two July ARM cases.
- The contributions by net radiation and latent heat flux on the atmospheric thermodynamic energy budget vary in the tropical cases, however. For the SCSMEX and GATE cases, the net radiation (cooling) is not negligible in the temperature budget; it is as large as 20% of the net condensation (moist convection interacts with the radiative processes). Net radiation is very small and does not contribute to the atmospheric temperature budget for the TOGA COARE cases. This is because thick anvil clouds are simulated in the TOGA COARE cases. However, the radiation process still plays an important role in the diurnal variability of rainfall for the TOGA COARE convective systems (Tao et al. 1996; Sui et al. 1998).
- Two different PEs were estimated using model results. The first, PE_1, is defined as the ratio between rainfall

and positive cloud condensation (condensation plus deposition), and the second, PE_2, is defined as the ratio between rainfall and the sum of rainfall and positive cloud condensation. The model results showed that the multiday mean PE varies from 32% to 45% (PE_1) and from 24% to 31% (PE_2) between the cloud systems from different geographic locations. Larger (or smaller) PE_1 is always associated with larger (or smaller) PE_2. The two SCSMEX cases, have identical PE and are the largest among all the simulations. The GATE case has the second largest PE. One of the TOGA COARE cases (10–17 December) and one of the ARM cases (12–17 July) have the smallest PE. It may be expected that the ARM (midlatitude, continental) and GATE cases would have lower PEs because they developed under drier environments. Generally, the model results suggest that there is no clear relationship between PE and rainfall, the net condensation, or the large-scale forcing. But, the model results suggest that cases with large, positive net condensation terms in the moist static energy budget tend to have a large PE.

- PE_2 and its relationship with the mass-weighted relative humidity are also examined using 6-hourly model data. The results indicate that PE is higher in moist versus drier environments in good agreement with Ferrier et al. (1996) and Shepherd et al. (2001). The model results also suggest PE is higher in moister mid- and upper-level environments for the TOGA COARE and SCSMEX cases. This result is in good agreement with Lucas et al. (2000). In addition, the model results suggest that there is no clear relationship between the PE and the total mass-weighted relative humidity or the middle and upper tropospheric moisture in these cases.
- PE_2 and its relationship with the vertical shear of the horizontal wind are also examined using 6-hourly model data. For one of the TOGA COARE (19–27 December) and one of the ARM (26–30 June) cases, the decrease in PE with increasing wind shear in these low to moderate shear regimes is generally in agreement with Weisman and Klemp (1982) and Shie et al. (2003). However, PE_2 increases with increasing low-level wind shear in GATE and other TOGA COARE cases. The increase in midlevel shear results in a lower PE for the TOGA COARE and GATE cases in agreement with Lucas et al. (2000). The correlation (based on the best polynomial fit) is quite weak however.
- The model results suggest that the GCE can underestimate the rainfall when a positive large-scale forcing is imposed/prescribed (except for the GATE case). More cloud ensemble modeling studies will be needed to generalize this relationship.

Real clouds and cloud systems are 3D. Two-dimensional CRMs today are applied in multiday integrations for computational reasons. Few 3D CEMs (e.g., Tao and Soong 1986; Tao et al. 1987; Lipps and Hemler 1986) have been used to study the response of clouds to large-scale forcing. In these 3D simulations, the model domain was small and integration times were between 3 and 6 h. Only recently, 3D experiments were performed for multiday periods for tropical cloud systems with large horizontal domains (Grabowski et al. 1998; Donner et al. 1999; Petch and Gray 2001; Xu et al. 2002, Tao 2003). Grabowski et al. (1998) and Tao (2003) found that cloud statistics, as well as surface precipitation and latent heating profiles, are very similar between the multiday 2D and 3D simulations for GATE and TOGA COARE cases. The reason for the strong similarity between the 2D and 3D CRM simulations is that the same observed (time varying) large-scale advective tendencies of potential temperature, water vapor mixing ratio, and horizontal momentum were used as the main forcing in both the 2D and 3D models. The 3D GCE model has recently been used to simulate ARM, SCSMEX, and other cases, and the results will be reported in a publication in the near future.

Khain et al. (1999) and Phillips et al. (2001, 2002) employed a 2D CRM with detailed, spectral-bin microphysics to examine precipitation formation and cloud–aerosol interactions associated with isolated clouds with short model integrations (a few hours). Their results clearly indicated that the precipitation processes are very sensitive to the concentration of aerosol particles (APs). In the case of a high (low) concentration of APs, warm rain is less (more) intense with smaller (larger) graupel and ice crystals. The bulk microphysics used in the model for this study does not allow cloud–aerosol interaction. An explicit, spectral-bin microphysics scheme developed by Khain et al. (2000) was implemented into the 2D version of the GCE model. Preliminary results suggest that the atmospheric aerosol concentration can have a significant impact on cloud and precipitation processes as shown in Khain et al. (1999) and Philips et al. (2001, 2002). The improved model will be used to study the sensitivity of atmospheric aerosol concentration on cloud and precipitation processes associated with clouds/cloud systems in very different large-scale environments (such as the present study). The sensitivity of microphysics (bulk versus detailed) on PE will be presented in a future paper.

Acknowledgments. This work is mainly supported by the NASA Headquarters Atmospheric Dynamics and Thermodynamics Program and the NASA Tropical Rainfall Measuring Mission (TRMM). The authors are grateful to Dr. R. Kakar at NASA headquarters for his support of this research. This research was also supported by the Office of Science (BER), U.S. Department of Energy, Interagency Agreement DE-AI02-04ER63755. The authors thank three anonymous reviewers for their constructive comments and Mr. S. Lang for reading the manuscript. Acknowledgment is also made to the NASA–Goddard Space Flight Center for computer time used in this research.

REFERENCES

Anthes, R. A., 1977: A cumulus parameterization scheme utilizing a one-dimensional cloud model. *Mon. Wea. Rev.*, **105,** 270–286.

Braham, R. R., Jr., 1952: The water and energy budgets of the thunderstorm and their relation to thunderstorm development. *J. Meteor.*, **9,** 227–242.

Chong, M., and D. Hauser, 1989: A tropical squall line observed during the COPT 81 Experiment in West Africa. Part II: Water budget. *Mon. Wea. Rev.*, **117,** 728–744.

Cotton, W. R., and G. J. Tripoli, 1978: Cumulus convection in shear flow—Three-dimensional numerical experiments. *J. Atmos. Sci.*, **35,** 1053–1521.

Das, S., D. Johnson, and W.-K. Tao, 1999: Single-column and cloud ensemble model simulations of TOGA COARE convective systems. *J. Meteor. Soc. Japan*, **77,** 803–826.

Donner, L. J., C. J. Seman, and R. S. Hemler, 1999: Three-dimensional cloud-system modeling of GATE convection. *J. Atmos. Sci.*, **56,** 1885–1912.

Fairall, C., E. F. Bradley, D. P. Rogers, J. B. Edson, and G. S. Young, 1996: Bulk parameterization of air-sea fluxes for TOGA COARE. *J. Geophy. Res.*, **101,** 3747–3764.

Fankhauser, J. C., 1988: Estimates of thunderstorm precipitation efficiency from field measurements in CCOPE. *Mon. Wea. Rev.*, **116,** 663–684.

Ferrier, B. S., J. Simpson, and W.-K. Tao, 1996: Factors responsible for different precipitation efficiencies between midlatitude and tropical squall simulations. *Mon. Wea. Rev.*, **124,** 2100–2125.

Fovell, R. G., and Y. Ogura, 1988: Numerical simulation of a midlatitude squall line in two dimensions. *J. Atmos. Sci.*, **45,** 3846–3879.

Fritsch, J. M., and C. F. Chappell, 1980: Numerical prediction of convectively driven mesoscale pressure systems. Part I: Convective parameterization. *J. Atmos. Sci.*, **37,** 1722–1733.

Gamache, J. F., and R. A. Houze Jr., 1983: Water budget of a mesoscale convective system in the Tropics. *J. Atmos. Sci.*, **40,** 1835–1850.

Grabowski, W. W., X. Wu, and M. W. Moncrieff, 1996: Cloud-resolving modeling of cloud systems during Phase III of GATE. Part I. Two-dimensional experiments. *J. Atmos. Sci.*, **53,** 3684–3709.

——, ——, ——, and W. D. Hall, 1998: Cloud-resolving modeling of cloud systems during Phase III of GATE. Part II: Effects of resolution and the third spatial dimension. *J. Atmos. Sci.*, **55,** 3264–3282.

Grell, G. A., 1993: Prognostic evaluation of assumptions used by cumulus parameterizations. *Mon. Wea. Rev.*, **121,** 764–787.

Johnson, D., W.-K. Tao, J. Simpson, and C.-H. Sui, 2002: A study of the response of deep tropical clouds to large-scale processes. Part I: Model set-up strategy and comparison with observation. *J. Atmos. Sci.*, **59,** 3492–3518.

Johnson, R. H., and P. E. Ciesielski, 2002: Characteristics of the 1998 summer monsoon onset over the northern South China Sea. *J. Meteor. Soc. Japan*, **80,** 561–578.

Khain, A. P., A. Pokrovsky, and I. Sednev, 1999: Some effects of cloud–aerosol interaction on cloud microphysics structure and precipitation formation: Numerical experiments with a spectral microphysics cloud ensemble model. *Atmos. Res.*, **52,** 195–220.

——, M. Ovtchinnikov, M. Pinsky, A. Pokrovsky, and H. Krugliak, 2000: Notes on the state-of-the-art numerical modeling of cloud microphysics. *Atmos. Res.*, **55,** 159–224.

Klemp, J. B., and R. Wilhelmson, 1978: The simulation of three-dimensional convective storm dynamics. *J. Atmos. Sci.*, **35,** 1070–1096.

Krueger, S. K., 1988: Numerical simulation of tropical cumulus clouds and their interaction with the subcloud layer. *J. Atmos. Sci.*, **45,** 2221–2250.

Lau, K. M., and Coauthors, 2000: A report of the field operations and early results of the South China Sea Monsoon experiment (SCSMEX). *Bull. Amer. Meteor. Soc.*, **81,** 1261–1270.

Li, X., C.-H. Sui, K.-M. Lau, and M.-D. Chou, 1999: Large-scale forcing and cloud–radiation interaction in the tropical deep convective regime. *J. Atmos. Sci.*, **56,** 3028–3042.

Lilly, D. K., 1975: Severe storms and storm systems: Scientific background, methods and critical questions. *Pure Appl. Geophys.*, **113,** 713–734.

Lin, X., and R. H. Johnson, 1996: Heating, moistening and rainfall over the western Pacific during TOGA COARE. *J. Atmos. Sci.*, **53,** 3367–3383.

Lin, Y.-L., R. D. Farley, and H. D. Orville, 1983: Bulk parameterization of the snow field in a cloud model. *J. Climate Appl. Meteor.*, **22,** 1065–1092.

Lipps, F. B., and R. S. Helmer, 1986: Numerical simulation of deep tropical convection associated with large-scale convergence. *J. Atmos. Sci.*, **43,** 1796–1816.

Lucas, C., E. J. Zipser, and B. S. Ferrier, 2000: Sensitivity of tropical west Pacific oceanic squall lines to temperature, wind and moisture profiles. *J. Atmos. Sci.*, **57,** 2351–2373.

Malkus, J. S., 1957: Trade cumulus cloud groups: Some observations suggesting a mechanism of their origin. *Tellus*, **9,** 33–44.

Moncrieff, M. W., 1981: A theory of organized steady convection and its transport properties. *Quart. J. Roy. Meteor. Soc.*, **107,** 29–50.

——, S. K. Krueger, D. Gregory, J.-L. Redelsperger, and W.-K. Tao, 1997: GEWEX Cloud System Study (GCSS) Working Group 4: Precipitating convective cloud systems. *Bull. Amer. Meteor. Soc.*, **78,** 831–845.

Oury, S., X. Dou, and J. Testud, 2000: Estimate of precipitation from the dual-beam airborne radars in TOGA COARE. Part II: Precipitation efficiency in the 9 February 1993 MCS. *J. Appl. Meteor.*, **39,** 2371–2384.

Petch, J. C., and M. E. B. Gray, 2001: Sensitivity studies using a cloud-resolving model simulation of the tropical west Pacific. *Quart. J. Roy. Meteor. Soc.*, **127,** 2287–2306.

Phillips, T. W., A. M. Blyth, and P. R. A. Brown, 2001: The glaciation of a cumulus cloud over New Mexico. *Quart. J. Roy. Meteor. Soc.*, **127,** 1513–1534.

——, T. W. Choularton, A. M. Blyth, and J. Latham, 2002: The influence of aerosol concentrations on the glaciation and precipitation of a cumulus cloud. *Quart. J. Roy. Meteor. Soc.*, **128,** 951–971.

Rutledge, S. A., and P. V. Hobbs, 1984: The mesoscale and microscale structure and organization of clouds and precipitation in midlatitude clouds. Part XII: A diagnostic modeling study of precipitation development in narrow cold frontal rainbands. *J. Atmos. Sci.*, **41,** 2949–2972.

Shepherd, J. M., B. S. Ferrier, and P. S. Ray, 2001: Rainfall morphology in Florida convergence zones: A numerical study. *Mon. Wea. Rev.*, **129,** 177–197.

Shie, C.-L., W.-K. Tao, J. Simpson, and C.-H. Sui, 2003: Quasi-equilibrium states in the Tropics simulated by a cloud-resolving model. Part I: Specific features and budget analysis. *J. Climate*, **5,** 817–833.

Smolarkiewicz, P. K., and W. W. Grabowski, 1990: The multidimensional positive advection transport algorithm: Nonoscillatory option. *J. Comput. Phys.*, **86,** 355–375.

Soong, S.-T., and Y. Ogura, 1980: Response of tradewind cumuli to large-scale processes. *J. Atmos. Sci.*, **37,** 2035–2050.

——, and W.-K. Tao, 1980: Response of deep tropical clouds to mesoscale processes. *J. Atmos. Sci.*, **37,** 2016–2036.

——, and ——, 1984: A numerical study of the vertical transport of momentum in a tropical rainband. *J. Atmos. Sci.*, **41,** 1049–1061.

Sui, C.-H., and M. Yanai, 1986: Cumulus ensemble effects on the large-scale vorticity and momentum fields of GATE. Part I: Observational evidence. *J. Atmos. Sci.*, **43,** 1618–1642.

——, K.-M. Lau, and X. Li, 1998: Convective–radiative interaction in simulated diurnal variations of tropical cumulus ensemble. *J. Atmos. Sci.*, **55,** 2345–2357.

Tao, W.-K., 2003: Goddard Cumulus Ensemble (GCE) model: Application for understanding precipitation processes. *Cloud Sys-*

tems, Hurricanes and the Tropical Rainfall Measuring Mission (TRMM): A Tribute to Dr. Joanne Simpson, Meteor. Monogr., No. 51, Amer. Meteor. Soc., 103–138.

——, and J. Simpson, 1984: Cloud interactions and merging: Numerical simulations. *J. Atmos. Sci.,* **41,** 2901–2917.

——, and S.-T. Soong, 1986: A study of the response of deep tropical clouds to mesoscale processes: Three-dimensional numerical experiments. *J. Atmos. Sci.,* **43,** 2653–2676.

——, and J. Simpson, 1989: Modeling study of a tropical squall-type convective line. *J. Atmos. Sci.,* **46,** 177–202.

——, and ——, 1993: The Goddard Cumulus Ensemble Model. Part I: Model description. *Terr. Atmos. Oceanic Sci.,* **4,** 19–54.

——, ——, and S.-T. Soong, 1987: Statistical properties of a cloud ensemble: A numerical study. *J. Atmos. Sci.,* **44,** 3175–3187.

——, J. Scala, B. Ferrier, and J. Simpson, 1995: The effects of melting processes on the development of a tropical and a mid-latitudes squall line. *J. Atmos. Sci.,* **52,** 1934–1948.

——, J. Simpson, S. Lang, C.-H. Sui, B. Ferrier, and M.-D. Chou, 1996: Mechanisms of cloud–radiation interaction in the Tropics and midlatitudes. *J. Atmos. Sci.,* **53,** 2624–2651.

——, S. Lang, J. Simpson, W. S. Olson, D. Johnson, B. Ferrier, C. Kummerow, and R. Adler, 2000: Vertical profiles of latent heat release and their retrieval in TOGA COARE convective systems using a cloud resolving model, SSM/I and radar data. *J. Meteor. Soc. Japan,* **78,** 333–355.

——, C.-L. Shie, D. Johnson, R. Johnson, S. Braun, J. Simpson, and P. E. Ciesielski, 2003a: Convective systems over South China Sea: Cloud-resolving model simulations. *J. Atmos. Sci.,* **60,** 2929–2956.

——, and Coauthors, 2003b: Microphysics, radiation and surface processes in a non-hydrostatic model. *Meteor. Atmos. Phys.,* **82,** 97–137.

Wang, Y., W.-K. Tao, and J. Simpson, 1996: The impact of ocean surface fluxes on a TOGA COARE cloud system. *Mon. Wea. Rev.,* **124,** 2753–2763.

Weisman, M. L., and J. B. Klemp, 1982: The dependence of numerically simulated convective storms on vertical wind shear and buoyancy. *Mon. Wea. Rev.,* **110,** 504–520.

Wilhelmson, R. B., and J. B. Klemp, 1978: A numerical study of storm splitting that leads to long-lived storms. *J. Atmos. Sci.,* **35,** 1975–1986.

Wu, X., W. W. Grabowski, and M. W. Moncrieff, 1998: Long-term behavior of cloud systems in TOGA COARE and their interactions with radiative and surface processes. Part I: Two-dimensional modeling study. *J. Atmos. Sci.,* **55,** 2693–2714.

——, ——, and ——, 1999: Long-term behavior of cloud systems in TOGA COARE and their interactions with radiative and surface processes. Part II: Effects of the ice microphysics on cloud–radiation interaction. *J. Atmos. Sci.,* **56,** 3177–3195.

Xie, S. C., R. T. Cederwall, J. J. Yio, and K. M. Xu, 2001: Intercomparison and evaluation of cumulus parameterizations under summertime mid-latitude continental conditions. *Proc. 11th ARM Science Team Meeting,* Atlanta, GA, U.S. Department of Energy, Atmospheric Radiation Measurement, 1095–1135.

Xu, K.-M., and D. A. Randall, 1996: Explicit simulation of cumulus ensembles with the GATE Phase III data: Comparison with observations. *J. Atmos. Sci.,* **53,** 3709–3736.

——, and Coauthors, 2002: Intercomparison of cloud-resolving models with the ARM Summer 1997 IOP data. *Quart. J. Roy. Meteor. Soc.,* **128,** 593–624.

Zhang, M.-H., and J. L. Lin, 1997: Constrained variational analysis of sounding data based on column-integrated budgets of mass, moisture, and momentum: Approach and application to ARM measurements. *J. Atmos. Sci.,* **54,** 1503–1524.